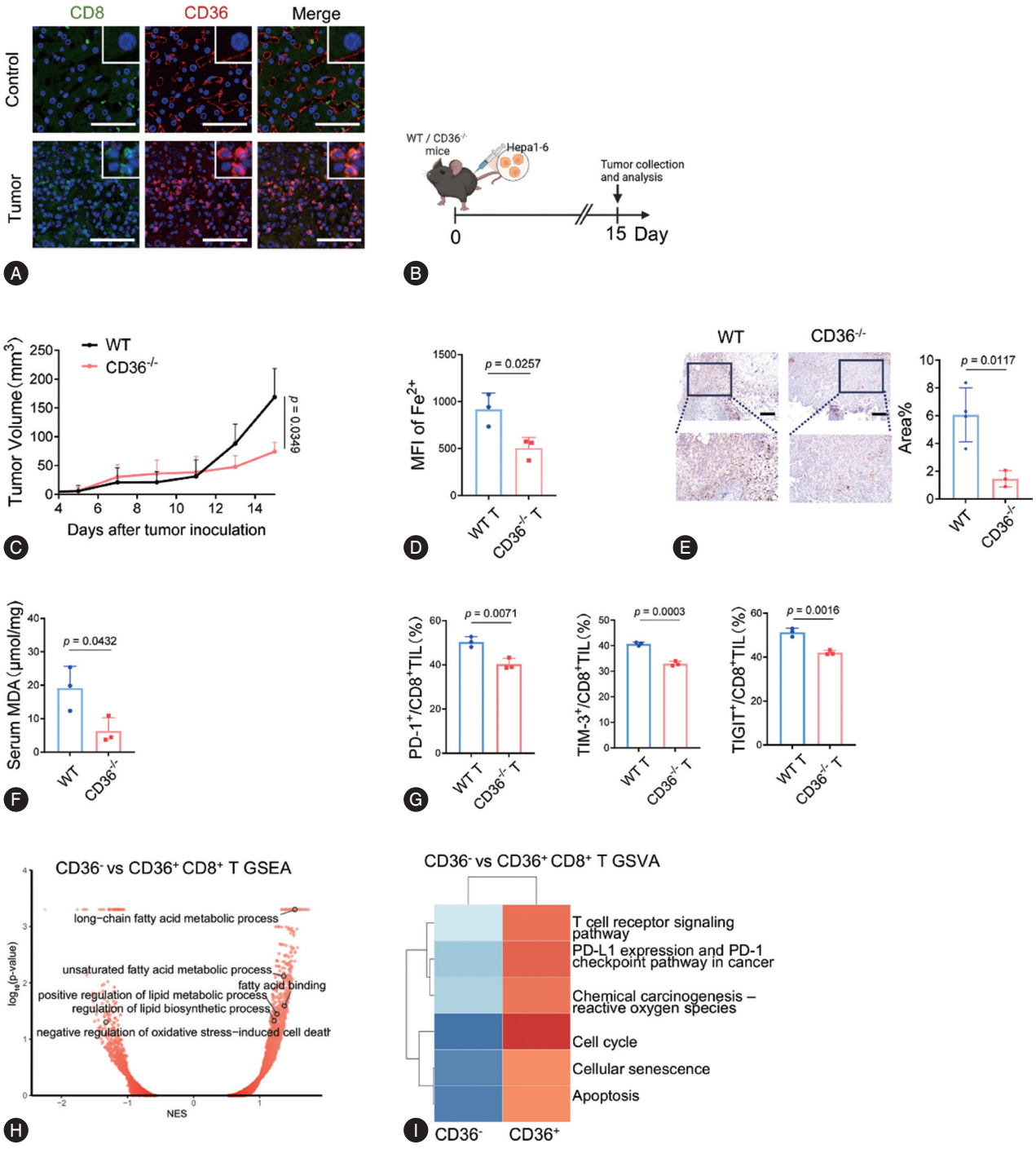

Supplementary Figure 14. CD36 deficiency rescues the CD8$^+$ T cells effector functions through reducing the iron accumulation. (A) mIHC staining of CD8 and CD36 in early-stage HCC tissues and normal liver tissues. Scale bar: 50 μm. (B) Schematic diagram of tumor implantation in WT and CD36$^{-/-}$ mice. (C) WT and CD36$^{-/-}$ mice were implanted with Hepa1-6 cells as indicated, and tumor growth curves were shown. n=3 mice per condition. (D) Intracellular Fe^{2+} levels in tumor-infiltrating CD8$^+$ T cells from WT and CD36$^{-/-}$ mice. n=3 mice per condition. (E) Diaminobenzidine-enhanced Prussian blue iron staining and quantification in tumors of WT and CD36$^{-/-}$ mice. Areas with positive Prussian staining were quantified. n=3 mice per condition. Scale bar: 100 μm. (F) Serum MDA levels in WT and CD36$^{-/-}$ mice. n=3 mice per condition. (G) Percentages of PD-1$^+$, TIM-3$^+$, and TIGIT$^+$ cells in tumor-infiltrating CD8$^+$ T cells from WT and CD36$^{-/-}$ mice were detected by flow cytometry. n=3 mice per condition. (H) Volcano plot showing GO terms enriched in CD36$^+$ CD8$^+$ T cells compared with CD36$^-$ CD8$^+$ T cells in the single-cell sequencing data of murine HTVi HCC. (I) GSVA showing enriched pathways in CD36$^+$ CD8$^+$ T cells compared with CD36$^-$ CD8$^+$ T cells.